CrossMark

JM PAPERS

Streamwise inclination angle of wall-attached eddies in turbulent channel flows

Cheng Cheng[1], Wei Shyy[1] and Lin Fu[1,2,3,†]

[1]Department of Mechanical and Aerospace Engineering, The Hong Kong University of Science and Technology, Clear Water Bay, Kowloon, Hong Kong

[2]Department of Mathematics, The Hong Kong University of Science and Technology, Clear Water Bay, Kowloon, Hong Kong

[3]Center for Ocean Research in Hong Kong and Macau (CORE), The Hong Kong University of Science and Technology, Clear Water Bay, Kowloon, Hong Kong

We develop a new methodology to assess the streamwise inclination angles (SIAs) of the wall-attached eddies populating the logarithmic region with a given wall-normal height. To remove the influences originating from other scales on the SIA estimated via two-point correlation, the footprints of the targeted eddies in the vicinity of the wall and the corresponding streamwise velocity fluctuations carried by them are isolated simultaneously, by coupling the spectral stochastic estimation with the attached-eddy hypothesis. Datasets produced with direct numerical simulations spanning $Re_\tau \sim O(10^2)$–$O(10^3)$ are dissected to study the Reynolds number effect. The present results show, for the first time, that the SIAs of attached eddies are Reynolds-number-dependent in low and medium Reynolds numbers, and tend to saturate at $45°$ as the Reynolds number increases. The mean SIA reported by vast previous experimental studies are demonstrated to be the outcomes of the additive effect contributed by multi-scale attached eddies. These findings clarify the long-term debate and perfect the picture of the attached-eddy model.

Key words: boundary layer structure, turbulence theory, turbulent boundary layers

1. Introduction

It is generally recognized that high-Reynolds-number wall-bounded turbulence is filled with coherent motions of disparate scales, which are responsible for energy transfer and
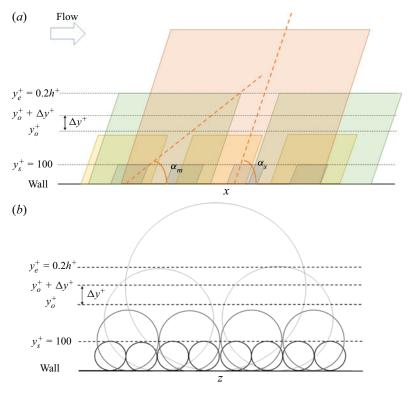
† Email address for correspondence: linfu@ust.hk

Figure 1. A schematic of the attached-eddy model: (*a*) *x*–*y* plane view, and (*b*) *y*–*z* plane view. Each parallelogram in (*a*) and circle in (*b*) represents an individual attached eddy. Here, *x*, *y* and *z* denote the streamwise, wall-normal and spanwise directions, respectively. Also, y_s^+ (= 100) and y_e^+ (= $0.2h^+$) denote the lower and upper bounds of the logarithmic region, respectively (Jiménez 2018; Baars & Marusic 2020*a*; Wang, Hu & Zheng 2021); y_o^+ is the outer reference height; Δy^+ is the local grid spacing along the wall-normal direction; and α_m and α_s are the mean and individual SIA of attached eddies, respectively. These two diagrams are merely conceptual sketches, and the eddy population density is not in accordance with that of Perry & Chong (1982).

the fluctuation generation of turbulence. Until now, the most elegant conceptual model describing these energy-containing motions has been the attached-eddy model (Townsend 1976; Perry & Chong 1982). It hypothesizes that the logarithmic region is occupied by an array of randomly distributed and self-similar energy-containing motions (or eddies) with their roots attached to the near-wall region (see figure 1). During recent decades, a growing body of evidence that supports the attached-eddy hypothesis has emerged rapidly, e.g. Hwang (2015), Hwang & Sung (2018), Cheng *et al.* (2020*b*), Hwang, Lee & Sung (2020), to name a few. The reader is referred to a recent review work by Marusic & Monty (2019) for more details. Throughout the paper, the terms 'eddy' and 'motion' are exchangeable. It should be noted that the terms 'wall-attached motions' and 'wall-attached eddies' used in the present study refer to not only the self-similar eddies in the logarithmic region, but also the very-large-scale motions (VLSMs) or superstructures, as some recent studies have shown that VLSMs are also wall-attached, despite their physical characteristics not matching the attached-eddy model (Hwang & Sung 2018; Yoon *et al.* 2020).

Previous studies have established that the energy-containing eddies populating the logarithmic and outer regions bear characteristic streamwise inclination angles (SIAs) due to the mean shear (see figure 1*a*). As early as the 1970s, Kovasznay, Kibens &

Blackwelder (1970) found that the large-scale structures in the outer intermittent region of a turbulent boundary layer have a moderate tilt in the streamwise direction. On the other hand, for the eddies in the logarithmic region of wall turbulence, the wall-attached Λ-vortex was used by Perry & Chong (1982) to illustrate them. According to Adrian, Meinhart & Tomkins (2000), these Λ-vortices are apt to cluster along the flow direction and form an integral whole (generally called vortex packets). Further observations in channel flows (Christensen & Adrian 2001) demonstrated that the heads of Λ-vortices among the vortex packets tend to slope away from the wall in a statistical sense, with SIAs between $12°$ and $13°$. Most additional studies have shown a similar result, and it is accepted widely that the approximate SIAs of eddies are in the range $10°$–$16°$ (Boppe, Neu & Shuai 1999; Christensen & Adrian 2001; Carper & Porté-Agel 2004; Marusic & Heuer 2007; Baars, Hutchins & Marusic 2016). Besides, the SIA is also found to be Reynolds-number-independent (Marusic & Heuer 2007).

However, the SIA estimated by experimentalists using the traditional statistical approach is indeed the mean structure angle (Marusic & Heuer 2007; Deshpande, Monty & Marusic 2019). The common procedure to obtain the SIA is based on the calculation of the cross-correlation between the streamwise wall-shear stress fluctuation (τ_x') and the streamwise velocity fluctuation (u') at a wall-normal position in the log region (y_o). The cross-correlation can be expressed as

$$R_{\tau_x' u'}(\Delta x) = \frac{\langle \tau_x'(x)\, u'(x + \Delta x, y_o)\rangle}{\sqrt{\langle \tau_x'^2\rangle \langle u'^2\rangle}}, \tag{1.1}$$

where $\langle \cdot \rangle$ represents the ensemble temporal and spatial average, and Δx is the streamwise delay. The SIA can be estimated by

$$\alpha_m = \arctan\left(\frac{y_o}{\Delta x_p}\right), \tag{1.2}$$

where Δx_p denotes the streamwise delay corresponding to the peak in $R_{\tau_x' u'}$. Considering that an array of wall-attached eddies with distinct wall-normal heights can convect simultaneously past the reference position y_o, α_m in (1.2) should be regarded as the mean angle of these eddies. Hence the subscript m in (1.2) refers to 'mean'.

To estimate the SIAs of the largest wall-attached eddies, Deshpande *et al.* (2019) introduced a spanwise offset between the near-wall and logarithmic probes to isolate these wall-attached motions in the log region. They found that their SIAs are approximately $45°$. This observation is consistent with several theoretical analyses. For example, Moin & Kim (1985) and Perry, Uddin & Marusic (1992) proposed that for flows with two-dimensional mean flows, the characteristic angles of the energy-containing eddies should follow the direction of the principal rate of mean strain. More specifically, their SIAs should be $45°$ for a zero-pressure-gradient turbulent boundary layer (Perry *et al.* 1992). Marusic (2001) found that the mean SIA of the induced turbulence field by attached eddies is akin to the experimental measurements if the hierarchical attached eddies tilt away from the wall with individual SIA $45°$ and organize like the vortex packets observed in numerical and laboratory experiments.

Reviewing the work of predecessors, it can be found that the SIAs of attached eddies at a given length scale are ambiguous. Traditional measurements are applicable only for the assessment of the mean SIA (Brown & Thomas 1977; Boppe *et al.* 1999; Marusic & Heuer 2007). Moreover, the technique adopted by Deshpande *et al.* (2019) can isolate only

Case	Re_τ	$L_x(h)$	$L_y(h)$	$L_z(h)$	Δx^+	Δz^+	Δy^+_{min}	Δy^+_{max}	N_F	Tu_τ/h
Re550	547	8π	2	4π	13.4	6.8	0.04	6.7	142	22
Re950	934	8π	2	3π	11.5	5.7	0.03	7.6	73	12
Re2000	2003	8π	2	3π	12.3	6.2	0.32	8.9	48	11
Re4200	4179	2π	2	π	12.3	6.2	0.32	10.6	40	15

Table 1. Parameter settings of the DNS database. Here, L_x, L_y and L_z are the sizes of the computational domain in the streamwise, wall-normal and spanwise directions, respectively. Also, Δx^+ and Δz^+ denote the streamwise and spanwise grid resolutions in viscous units, respectively; Δy^+_{min} and Δy^+_{max} denote the finest and coarsest resolutions in the wall-normal direction, respectively; N_F and Tu_τ/h indicate the number of instantaneous flow fields and the total eddy turnover time used to accumulate statistics, respectively.

the largest wall-attached motions in the logarithmic region. Considering the characteristic scale of an individual attached eddy as its wall-normal height, as per the attached-eddy model (Townsend 1976; Perry & Chong 1982), it is self-evident that it is of great importance to assess the SIAs of attached eddies with any heights in the logarithmic region, for not only the completeness of attached-eddy hypothesis, but also the accuracy of turbulence simulations (Marusic 2001; Carper & Porté-Agel 2004). In the present study, we aim to achieve this goal by leaning upon the modified spectral stochastic estimation (SSE) proposed by Baars *et al.* (2016), and dissecting the direct numerical simulations (DNS) database spanning broad-band Reynolds numbers. We will also discuss the relationship between the mean SIA and the scale-based SIA.

2. DNS database and methodology to calculate the SIA

2.1. *DNS database*

The DNS database adopted in the present study has been validated extensively by Jiménez and co-workers (Del Álamo & Jiménez 2003; Del Álamo *et al.* 2004; Hoyas & Jiménez 2006; Lozano-Durán & Jiménez 2014). Four cases, at $Re_\tau = 545$, 934, 2003 and 4179, are used and named Re550, Re950, Re2000 and Re4200, respectively ($Re_\tau = hu_\tau/\nu$, where h denotes the channel half-height, u_τ the wall friction velocity and ν the kinematic viscosity). All these data are provided by the Polytechnic University of Madrid. Details of the parameter settings are listed in table 1. Note that the relatively smaller computational domain size of Re4200 may influence the estimation of SIAs of the attached eddies populating the upper part of the logarithmic region. This limitation will be discussed in § 3 and the Appendix.

2.2. *Spectral stochastic estimation*

According to the inner–outer interaction model (Marusic, Mathis & Hutchins 2010), large-scale motions would exert footprints on the near-wall region, i.e. the superposition effects. Baars *et al.* (2016) demonstrated that this component (denoted as $u_L'^+(x^+, y^+, z^+)$) can be obtained by the SSE of the streamwise velocity fluctuation at the logarithmic region y_o^+, namely by

$$u_L'^+\left(x^+, y^+, z^+\right) = F_x^{-1}\left\{H_L\left(\lambda_x^+, y^+\right) F_x\left[u_o'^+\left(x^+, y_o^+, z^+\right)\right]\right\}, \tag{2.1}$$

where $u_o'^+$ is the streamwise velocity fluctuation at y_o^+ in the logarithmic region, and F_x and F_x^{-1} denote the fast Fourier transform (FFT) and the inverse FFT in the streamwise

direction, respectively. Here, H_L is the transfer kernel, which evaluates the correlation between $\widehat{u'}(y^+)$ and $\widehat{u'_o}(y_o^+)$ at a given length scale λ_x^+; it can be calculated as

$$H_L\left(\lambda_x^+, y_o^+\right) = \frac{\left\langle \widehat{u'}\left(\lambda_x^+, y^+, z^+\right) \overline{\widehat{u'_o}}\left(\lambda_x^+, y_o^+, z^+\right)\right\rangle}{\left\langle \widehat{u'_o}\left(\lambda_x^+, y_o^+, z^+\right) \overline{\widehat{u'_o}}\left(\lambda_x^+, y_o^+, z^+\right)\right\rangle}, \tag{2.2}$$

where $\widehat{u'}$ is the Fourier coefficient of u', and $\overline{\widehat{u'}}$ is the complex conjugate of $\widehat{u'}$. Here, y^+ is set as $y^+ = 0.3$, and the outer reference height y_o^+ varies from 100 to the outer region $0.7h^+$ according to the wall-normal grid distribution. Once $u_L'^+$ is obtained, the superposition component of $\tau_x'^+$ can be calculated by definition (i.e. $\partial u_L'^+/\partial y^+$ at the wall) and denoted as $\tau_{x,L}'^+(y_o^+)$.

Analogously, to eliminate the effects from the wall-detached eddies with random orientations, which contribute significantly to the streamwise velocity fluctuations at y_o^+, we can also use the near-wall streamwise velocity fluctuation in the viscous layer y^+ to reconstruct the wall-coherent streamwise velocity fluctuation in the logarithmic region y_o^+ by SSE (Adrian 1979), i.e.

$$u_W'^+\left(x^+, y_o^+, z^+\right) = F_x^{-1}\left\{H_W\left(\lambda_x^+, y^+\right) F_x\left[u'^+\left(x^+, y^+, z^+\right)\right]\right\}, \tag{2.3}$$

where $u_W'^+$ is the wall-coherent component of $u_o'^+$. The wall-based transfer kernel H_W can be calculated as

$$H_W\left(\lambda_x^+, y_o^+\right) = \frac{\left\langle \widehat{u'_o}\left(\lambda_x^+, y_o^+, z^+\right) \overline{\widehat{u'}}\left(\lambda_x^+, y^+, z^+\right)\right\rangle}{\left\langle \widehat{u'}\left(\lambda_x^+, y^+, z^+\right) \overline{\widehat{u'}}\left(\lambda_x^+, y^+, z^+\right)\right\rangle}. \tag{2.4}$$

Figure 2(*a*) shows the variation of $\langle u_W'^{2+}\rangle$ as a function of y_o/h in the case Re2000. The full-channel data are included for comparison. It can be seen that $\langle u_W'^{2+}\rangle$ follows roughly the logarithmic decay for $0.09 \le y_o/h \le 0.2$, i.e. the logarithmic region. To quantify the logarithmic decay systematically, we define the indicator function $\varXi = y(\partial\langle u'^{2+}\rangle/\partial y)$, and display its variations in figure 2(*b*). Comparing with the full-channel data, a comparatively well-defined plateau is observed for $\langle u_W'^{2+}\rangle$. The logarithmic variance of $\langle u_W'^{2+}\rangle$ shown in figure 2 is the consequence of the additive attached eddies (Townsend 1976), and can be expressed as

$$\langle u_W'^{2+}\rangle = C_2 - C_1 \ln(y_o/h), \tag{2.5}$$

where C_2 and C_1 are two constants, and C_1 is approximately equal to 0.54. Actually, the magnitude of the slope of the logarithmic decaying is affected by the Reynolds number, the configuration of the wall turbulence, the methodology for isolating the signals carried by the attached eddies, and the effects of the VLSMs. The indicator function $\varXi$ of the full-channel data shown in figure 2(*b*) suggests that the logarithmic region of case Re2000 is not fully developed, as the slope value of the logarithmic decaying is smaller than the Townsend–Perry constant 1.26 reported in high-Reynolds-number experiments (Marusic *et al.* 2013), and close to the magnitude of C_1 observed here. Furthermore, Baars & Marusic (2020*b*) reported that $C_1 = 0.98$ in turbulent boundary layers by analysing the streamwise velocity fluctuations carried by the attached eddies in the logarithmic region, while Hu, Yang & Zheng (2020) and Hwang *et al.* (2020) showed that $C_1 = 0.8$ and 0.37 in channel flows, respectively. Hu *et al.* (2020) adopted a scale-based filter to
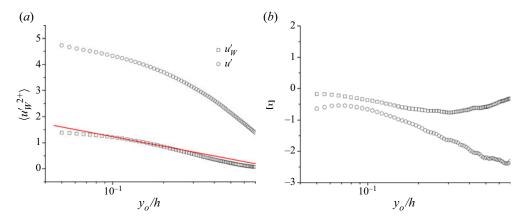
Figure 2. (*a*) Variations of the statistic $\langle u_W'^{2+}\rangle$ as a function of y_o/h, with the full-channel data $\langle u'^{2+}\rangle$ included for comparison. (*b*) Variations of the indicator function $\varXi$ as functions of y_o/h. The red line in (*a*) denotes the logarithmic decaying (2.5) with $C_1 = 0.54$. The data is taken from the case Re2000.
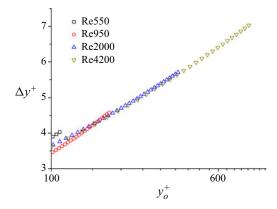

Figure 3. Variations of Δy^+ as functions of y_o^+ in the logarithmic region for all cases.

extract the streamwise velocity fluctuations associated with the attached eddies in the logarithmic region, and did not take into account their imperfect coherence with the near-wall flow at each scale. The wall-based transfer kernel H_W in (2.4) employed here can achieve this. Hwang *et al.* (2020) utilized the three-dimensional clustering method to identify the wall-attached structures in a channel flow. The differences among these decomposition methodologies may be the reason why the magnitude of C_1 for turbulent channel flows reported by Hu *et al.* (2020) and Hwang *et al.* (2020) is not identical to that of the present study. Besides, it is noted that the effects of VLSMs are also retained in $\langle u_W'^{2+}\rangle$, and their impacts on the logarithmic decaying are non-negligible. By the way, the methodology introduced in § 2.3 to estimate the SIAs of attached eddies at a single scale can effectively diminish the effects originating from the VLSMs (see figure 4). In summary, these observations demonstrate that u_W' can be considered as approximately the streamwise velocity fluctuations carried by the multi-scale wall-attached eddies. We will focus on the statistics in the logarithmic region in the following sections.

2.3. *Methodology to isolate targeted eddies*

Apparently, the SIAs of attached eddies at a single scale (α_s) cannot be pursued by (1.1)–(1.2). It is worth noting that in (1.1)–(1.2), the input parameter and signals are y_o, τ_x'
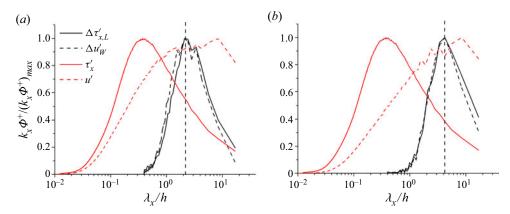
946 A49-6

Figure 4. Streamwise premultiplied spectra of $\Delta\tau'_{x,L}$, $\Delta u'_W$, τ'_x and u' for (*a*) $y_o = 0.1h$, and (*b*) $y_o = 0.2h$, in the case Re2000. Each spectrum is normalized with its maximum value. The vertical dashed lines are plotted to highlight the corresponding λ_x/h of the maximum values of the premultiplied spectra of $\Delta\tau'_{x,L}$ and $\Delta u'_W$.

and $u'(y_o)$. Thus to obtain an accurate α_s, y_o should be set reasonably, and τ'_x and $u'(y_o)$ should also be processed properly, to characterize the properties of the attached eddies at the targeted scale. Our new approach is based on this understanding.

According to the hierarchical distribution of the multi-scale attached eddies in high-Reynolds-number wall turbulence (see figure 1(*b*), also figure 14 of Perry & Chong 1982), $\tau'^+_{x,L}(y^+_o)$ represents the superposition contributed from the wall-attached motions with their height larger than y^+_o. Thus, the difference value $\Delta\tau'^+_{x,L}(y^+_o) = \tau'^+_{x,L}(y^+_o) - \tau'^+_{x,L}(y^+_o + \Delta y^+)$ can be interpreted as the superposition contribution generated by the wall-attached eddies with their wall-normal heights between y^+_o and $y^+_o + \Delta y^+$. Here, $y^+_o + \Delta y^+$ is the location of the wall-normal grid cell adjacent to that at y^+_o, as Δy^+ is the local grid spacing along the wall-normal direction, in viscous units, determined by the simulation set-ups. A similar numerical framework has been verified by our previous study (Cheng & Fu 2022). Correspondingly, the difference value $\Delta u'^+_W(y^+_o) = u'^+_W(y^+_o) - u'^+_W(y^+_o + \Delta y^+)$ is the streamwise velocity fluctuation carried by attached eddies populating the region between y^+_o and $y^+_o + \Delta y^+$. In this way, the SIAs of these eddies can be assessed by

$$\alpha_s(y_m) = \arctan\left(\frac{y_m}{\Delta x_p}\right), \qquad (2.6)$$

where $y_m = (y_o + (y_o + \Delta y))/2$, and Δx_p is the streamwise delay associated with the peak of the cross-correlation

$$R_{LW}(\Delta x) = \frac{\langle \Delta\tau'^+_{x,L}(x, y^+_o)\, \Delta u'^+_W(x + \Delta x, y^+_o)\rangle}{\sqrt{\left\langle \Delta\tau'^{2+}_{x,L}\right\rangle \left\langle \Delta u'^{2+}_W\right\rangle}}. \qquad (2.7)$$

As the statistical characteristics of an individual attached eddy being self-similar with its wall-normal height as per the attached-eddy hypothesis (Townsend 1976), y_m is just the characteristic scale of the wall-attached motions within y^+_o and $y^+_o + \Delta y^+$. Figure 3 shows the variations of Δy^+ as functions of y^+_o in the logarithmic region for all cases. It can be seen that the maximum values of Δy^+ are less than 7 in the case Re4200. In this regard,

treating y_m as the mean height of the attached eddies populating the region between y_o and $y_o + \Delta y$ is reasonable, as the zone between y_o and $y_o + \Delta y$ is narrow compared to the spanning of the logarithmic region. The new procedure isolates the attached eddies at a given scale from the rest of the turbulence. The cross-correlation, i.e. (2.7), gets rid of the influences originated from other scales, and preserves the phase information of the wall-attached motions with wall-normal height y_m.

Finally, the critical assumptions of the present approach and its realization merit a discussion. Our methodology is based on the hierarchical distribution of the attached eddies, and the hypothesis that the characteristic velocity scales carried by the attached eddies with different wall-normal heights are identical with their scale interactions omitted. That is, the attached eddies in each hierarchy contribute equally to the streamwise wall-shear fluctuations on the wall surface and the streamwise turbulence intensity in the lower bound of the logarithmic region. Only in this way, both $\Delta \tau_{x,L}'^+$ and $\Delta u_W'^+$ reflect approximately the characteristics of the attached eddies at y_m. In fact, these assumptions are also the key elements when developing the attached-eddy model (Townsend 1976; Perry & Chong 1982; Woodcock & Marusic 2015; Yang, Marusic & Meneveau 2016; Mouri 2017; Yang & Lozano-Durán 2017), and some of them may be valid only in high-Reynolds-number wall turbulence. For example, the hierarchical distribution of the multi-scale attached eddies is prominent at high-Reynolds-number turbulence (De Silva, Marusic & Hutchins 2016; Cheng *et al.* 2019; Marusic & Monty 2019). However, when the DNS data listed in table 1 are utilized to study the characteristics of the attached eddies, the finite Reynolds number effects and the intricate scale interactions would take effect inevitably. Besides, the VLSMs, which cannot be depicted by the attached-eddy model, would also impose non-trivial impacts (Perry & Marusic 1995; Baars & Marusic 2020*a*; Hwang *et al.* 2020). Accordingly, the subtraction between $u_W'^+(y_o^+)$ and $u_W'^+(y_o^+ + \Delta y^+)$ cannot achieve a sharp cut-off at the targeted scale in the spectral space, and hereby the spectrum of $\Delta u_W'^+(y_o^+)$ would be comparatively small but not negligible at the smaller and larger scales of the targeted one. The finiteness of Δy^+ is another factor, which is worth attention in some scenarios. Due to the limitations of numerical simulation, Δy^+ is a finitely small quantity. When assessing the SIA of the attached eddies at a given wall-normal height, treating y_m^+ as their characteristic scales (therefore neglecting the effects of the narrow band between y^+ and $y^+ + \Delta y^+$) is acceptable, because Δy^+ is rather small compared to the spanning of the whole logarithmic region. The linear growth of the typical length scales of $\Delta \tau_{x,L}'^+$ and $\Delta u_W'^+$ shown in figure 6(*b*) can verify this validity. On the other hand, when the spectral characteristics of $\Delta u_W'^+$ are considered, $\Delta u_W'^+$ should be interpreted as the additive outcomes of the attached eddies with their wall-normal heights within y^+ and $y^+ + \Delta y^+$, strictly speaking. Under these circumstances, the spectral energy distribution that corresponds to the self-similar attached eddies within this range should be observed to peak around the dominant wavelength, and vary continuously and locally. The results shown in figure 5 confirm our proposition. Details will be discussed in the next section.

3. Results

Before investigating the SIAs of attached eddies, it is important to study the characteristic scales of $\Delta \tau_{x,L}'$ and $\Delta u_W'$ first. Figures 4(*a,b*) show their streamwise premultiplied spectra at $y_o = 0.1h$ and $y_o = 0.2h$, respectively, for Re2000. The spectra of τ_x' and u' of the full-channel data are also included for comparison. Each spectrum is normalized with its
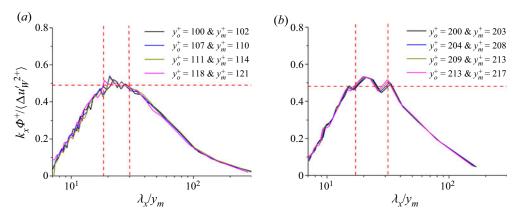
Figure 5. Premultiplied one-dimensional streamwise spectra of $\Delta u'_W$ around (a) $y_o = 0.05h$, (b) $y_o = 0.1h$, in Re2000. The horizontal dashed lines represent the plateaus or peaks of the spectra. The vertical lines are plotted to highlight the self-similar regions of each spectrum.
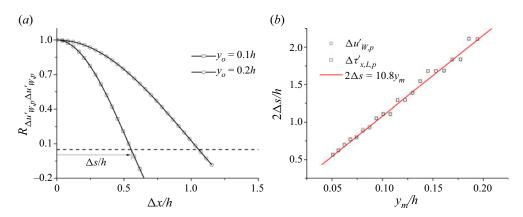

Figure 6. (a) Variations of $R_{\Delta u'_{W,p} \Delta u'_{W,p}}$ as functions of $\Delta x/h$ for two selected y_o. (b) Variations of $\Delta s/h$ as functions of y_m^+ for $\Delta \tau'^+_{x,L,p}$ and $\Delta u'^+_{W,p}$. The line in (b) denotes the linear variation $2\Delta s = 10.8 y_m$. The data is taken from the case Re2000.

maximum value. It can be seen that the spectra of $\Delta \tau'_{x,L}$ and $\Delta u'_W$ are roughly coincident, and peak at $\lambda_x = 2.1h$ for $y = 0.1h$, and $\lambda_x = 4.2h$ for $y = 0.2h$, respectively. By contrast, the spectra of τ'_x and u' do not share similar spectral characteristics. It is noted that $\Delta u'^2_W$ and $\Delta \tau'^2_{x,L}$ account for very little energy of the full-channel signals at the same wall-normal positions. For example, $\Delta u'^2_W$ at $y_o = 0.1h$ and $0.2h$ occupies 0.0034% and 0.002% of u'^2 at the corresponding positions, whereas $\Delta \tau'^2_{x,L}$ for $y_o = 0.1h$ and $0.2h$ occupies 0.012% and 0.0045% of τ'^2_x, respectively. Moreover, comparing with the spectra of the full-channel data, the spectra of $\Delta u'_W$ decay rapidly when $\lambda_x \geq 4h$ (see figure 4), which indicates that the effects of VLSMs on $\Delta u'_W$ are rather limited.

Figure 5 shows the streamwise premultiplied spectra of $\Delta u'_W$ around $y_o = 0.05h$ and $y_o = 0.1h$. Each spectrum is normalized by the energy of $\Delta u'_W$ at a given y_m. Clear plateau regions can be observed around the spectral peaks. For $y_o = 0.05h$, the region is $18 \leq \lambda_x/y_m \leq 30$, and for $y_o = 0.1h$ it is $17 \leq \lambda_x/y_m \leq 31$, which corresponds to the k_x^{-1} region in the spectrum predicated by the attached-eddy model, and can be considered

946 A49-9

as the spectral signatures of the attached eddies (Perry & Chong 1982; Perry, Henbest & Chong 1986; Hwang *et al.* 2020; Deshpande, Monty & Marusic 2021). Besides, the spectra shown here resemble the spectrum of the type A eddies hypothesized by Marusic & Perry (1995), i.e. the energy fraction captured by the attached-eddy model. These observations support the proposition that the $\Delta u'_W$ signals are the streamwise velocity fluctuations carried by the self-similar attached eddies predominantly. Moreover, they also indicate that the streamwise length scales of the dominant eddies increase with y_o, as the self-similar range is not altered significantly with increasing y_o.

To investigate further the scale characteristics of $\Delta \tau'_{x,L}$ and $\Delta u'_W$, we consider the autocorrelation function of $\Delta u'^{+}_{W,p}$ (the signals that are extracted from the spectral peaks shown in figure 5, i.e. filtered $\Delta u'_W$ with wavelength larger than $17 y_m$, but smaller than $31 y_m$), which takes the form

$$R_{\Delta u'_{W,p} \Delta u'_{W,p}}(\Delta x, y_o) = \frac{\langle \Delta u'_{W,p}(x, y_o, z) \, \Delta u'_{W,p}(x + \Delta x, y_o, z) \rangle}{\langle \Delta u'^2_{W,p}(x, y_o, z) \rangle}, \tag{3.1}$$

and the counterpart of $\Delta \tau'^{+}_{x,L}$ can be defined similarly. Figure 6(*a*) shows the variations of $R_{\Delta u'_{W,p} \Delta u'_{W,p}}$ as functions of $\Delta x/h$ for two selected y_o values. The larger y_o, the broader is $R_{\Delta u'_{W,p} \Delta u'_{W,p}}$. As a measure of the typical length scale, we employ $\Delta s/h$, which is the streamwise delay corresponding to $R_{\Delta u'_{W,p} \Delta u'_{W,p}} = 0.05$ or $R_{\Delta \tau'_{x,L,p} \Delta \tau'_{x,L,p}} = 0.05$ (here, 0.05 is an empirical small positive threshold). Figure 6(*b*) shows the variations of $2\Delta s/h$ as functions of y_m/h for $\Delta \tau'^{+}_{x,L,p}$ and $\Delta u'^{+}_{W,p}$. For both $\Delta \tau'^{+}_{x,L,p}$ and $\Delta u'^{+}_{W,p}$, $2\Delta s/h$ increases linearly with y_m/h throughout most of the logarithmic region. This observation is consistent with the attached-eddy hypothesis, which states that the length scales of the attached eddies grow linearly with their wall-normal heights (Hwang 2015; Marusic & Monty 2019). Moreover, both the streamwise length scales of $\Delta \tau'^{+}_{x,L,p}$ and $\Delta u'^{+}_{W,p}$ follow $2\Delta s = 10.8 y_m$ (considering the symmetry of the autocorrelation function with respect to $\Delta x = 0$, $2\Delta s$ truly represents the streamwise length scale of the signals). This scale characteristic agrees well with some previous studies. For example, Baars, Hutchins & Marusic (2017) showed that the streamwise/wall-normal aspect ratio of the wall-attached eddy structure is $\lambda_x/y = 14$ in turbulent boundary layers, which is close to the result here. Hwang *et al.* (2020) reported that the spectra of the self-similar wall-attached structures agree with the attached-eddy hypothesis at $\lambda_x = 12y$, which is consistent with the estimation of the present study. All these observations indicate that $\Delta \tau'^{+}_{x,L}$ and $\Delta u'^{+}_W$ are representative of the attached eddies at a certain wall-normal height, though the minor influences of VLSMs still exist, and treating y^{+}_m as their characteristic scales is reasonable.

In summary, all the observations mentioned above indicate that $\Delta \tau'_{x,L}$ and $\Delta u'_W$ are the outcomes of the energy-containing motions with the wall-normal heights approximately equal to y_m, and the cross-correlation, i.e. (2.7), truly reflects the phase difference between the streamwise velocity fluctuations carried by these motions and their footprints in the near-wall region. Other wall-normal positions and DNS cases yield similar results and are not shown here for brevity.

Figure 7(*a*) shows the variations of R_{LW} as functions of the streamwise delay for some selected wall-normal positions in the case Re2000. Since the streamwise length scales of the energy-containing motions are increased with their normal heights (see figure 4), R_{LW} becomes wider about the peak with increasing y_o. We can identify Δx_p obviously from the cross-correlation profiles, and the SIAs of the attached eddies at a given wall-normal height can be calculated according to (2.6). Figure 7(*b*) plots the variations
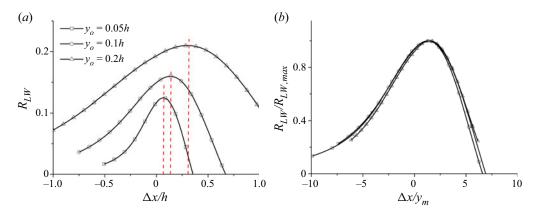
946 A49-10

Figure 7. (*a*) Variations of R_{LW}, i.e. the cross-correlation between $\Delta \tau_{x,L}'^{+}(y_o^+)$ and $\Delta u_W'^{+}(y_o^+)$, as functions of $\Delta x/h$ for some selected y_o values in the case Re2000. (*b*) Variations of the normalized R_{LW} as functions of $\Delta x/y_m$ for some selected y_o values in the case Re2000. The R_{LW} profiles are normalized with their maximum values in (*b*). The vertical dashed lines in (*a*) are plotted to highlight the maximum values of R_{LW} and their corresponding Δ_x/h.

of the normalized R_{LW} as functions of $\Delta x/y_m$ for some selected y_o in the case Re2000. The R_{LW} distributions are normalized with their maximum values $R_{LW,max}$. It can be seen that the profiles of $R_{LW}/R_{LW,max}$ for different wall-normal heights coincide well with each other, which indicates the self-similar characteristics of the energy-containing motions in the logarithmic region. We have checked that the correlations calculated from the raw data, i.e. $R_{\tau_x'u'}$ in (1.1), cannot coincide if normalized in this manner. Again, it demonstrates that the new methodology is capable of capturing the main properties of the attached eddies.

Figure 8 plots the variations of α_s as functions of y_m^+ for all cases; approximately, α_s increases from 27° for Re550, to 40° for Re4200. For a given case, α_s changes little spanning the logarithmic region except for the upper part of the logarithmic region in Re4200. Deshpande *et al.* (2019) isolated the large wall-attached structures in a DNS of turbulent boundary layer at $Re_\tau \approx 2000$, and found the corresponding SIAs to be 32° (see figure 4(*a*) of their paper). Their observation is consistent with the results of the present study. However, Deshpande *et al.* (2019) calculated only the SIAs of the largest wall-attached motions in the logarithmic region, due to the limitation of the methodology adopted in their study, whereas we make a thorough investigation on the SIAs of attached eddies with any wall-normal heights in the logarithmic region. Moreover, Deshpande *et al.* (2019) reported that the SIAs of the large wall-attached motions identified in a wind-tunnel boundary layer with $Re_\tau = 14000$ are approximately 50°. They ascribed the result difference between DNS and experiment to the limited streamwise scale range owing to the DNS domain size selected for analysis. Our results reveal that the Reynolds number effects play a non-negligible role in the formation of SIAs of attached eddies. To the authors' knowledge, this is the first time that the Reynolds number dependence of SIAs of the wall-attached motions at a given length scale has been shown clearly. Finally, it should be noted that α_s of Re4200 decreases rapidly for $y_m^+ > 500$ (not shown here). This diversity is due to the small computational domain size along the streamwise direction in this database. Thus in the discussion below, the statistics of α_s in the range $y_m^+ > 500$ in Re4200 will not be taken into account. The sensitivity of the presented results to the number of instantaneous flow fields employed for accumulating statistics is examined in the Appendix.
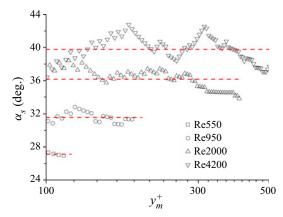
Figure 8. Variations of α_s as functions of y_m^+ for all cases. The red dashed lines denote the mean α_s across the logarithmic region of each case.
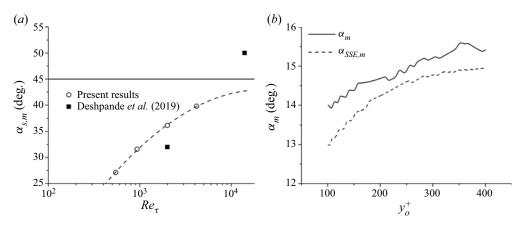

Figure 9. (*a*) Variations of the mean α_s ($\alpha_{s,m}$) statistic in the range of logarithmic region as a function of the friction Reynolds number; the experimental results of turbulent boundary layers (Deshpande *et al.* 2019) are also included for comparison. (*b*) Variations of α_m and $\alpha_{SSE,m}$ as functions of y_o^+ for Re2000. The solid black line in (*a*) denotes the theoretical prediction angle $45°$, and the dashed line in (*a*) indicates the asymptotic behaviour of $\alpha_{s,m}$.

Figure 9(*a*) shows the mean α_s ($\alpha_{s,m}$) distribution in the range of the logarithmic region as a function of the friction Reynolds number. It can be seen that the SIA may reach the theoretical prediction angle $45°$ (Perry *et al.* 1992) when $Re_\tau \sim O(10^4)$. The results of DNS of a turbulent boundary layer and wind-tunnel experiment of Deshpande *et al.* (2019) roughly agree with the tendency. The minor differences may result from the distinct configurations of the wall-bounded turbulence.

4. Discussion

4.1. *Effects of near-wall and detached motions*

To clarify the effects of near-wall and detached motions on the SIA assessment, we calculate the mean SIA based on the predictive signals, i.e.

$$\alpha_{SSE,m} = \arctan\left(\frac{y_o}{\Delta x_p}\right), \tag{4.1}$$

where Δx_p is the streamwise delay associated with the peak of the cross-correlation

$$R_{\tau'_{x,L} u'_W}(\Delta x) = \frac{\langle \tau'_{x,L}(x)\, u'_W(x + \Delta x, y_o) \rangle}{\sqrt{\langle \tau'^2_{x,L} \rangle \langle u'^2_W \rangle}}. \quad (4.2)$$

Figure 9(*b*) shows the variations of $\alpha_{SSE,m}$ as a function of y_o^+ for Re2000, and the statistics of α_m are also included for comparison. We can see that the $\alpha_{SSE,m}$ distribution is very closed to that of α_m. It highlights the fact that the phase information embedded in the raw signals $u'(y_o^+)$ and τ'_x is preserved by SSE. It also suggests that the near-wall and wall-detached motions, which cannot be captured by SSE, have a negligible impact on the magnitudes of SIA.

4.2. α_s *versus* α_m

Reviewing the approach to obtain the α_m (i.e. (1.1)–(1.2)), the proposition that α_m is the mean SIA of attached eddies manifests in three aspects. (1) the generation of τ'_x is not only the outcome of the near-wall motions, but also the footprints of all the wall-attached eddies (Cho, Hwang & Choi 2018; Cheng *et al.* 2020*a*). (2) In the logarithmic region, u' results from a sum of random contributions from the wall-attached eddies with distinct characteristic length scales (Yang *et al.* 2016), and a portion of contributions from the wall-detached eddies (Baars & Marusic 2020*b*). (3) Here, y_o is a wall-normal position located in the logarithmic region and chosen arbitrarily. As mentioned above, an array of wall-attached eddies with distinct wall-normal heights can convect simultaneously past this reference position.

Here, an additive SIA is calculated to highlight the relationship between α_s and α_m, namely,

$$\alpha_{add} = \arctan\left(\frac{y_s}{\Delta x_p}\right), \quad (4.3)$$

where $y_s^+ = 100$ is the lower boundary of the logarithmic region, and Δx_p is the streamwise delay associated with the peak of the cross-correlation

$$R_{add}(\Delta x) = \frac{\langle (\tau'^+_{x,L}(x, y_s^+) - \tau'^+_{x,L}(x, y_o^+))(u'^+_W(x + \Delta x, y_s^+) - u'^+_W(x + \Delta x, y_o^+)) \rangle}{\sqrt{\langle (\tau'^+_{x,L}(x, y_s^+) - \tau'^+_{x,L}(x, y_o^+))^2 \rangle \langle (u'^+_W(x, y_s^+) - u'^+_W(x, y_o^+))^2 \rangle}}, \quad (4.4)$$

where the reference position y_o^+ varies from $y_s^+ + \Delta y^+$ (equal to 104) to $0.7h^+$. Figure 10(*a*) shows the variations of α_{add} as a function of y_o^+ for Re2000. It can be seen that α_{add} decreases from $37.8°$ to $14°$ as y_o^+ increases, which corresponds to $\alpha_s(y_m^+ = 102)$ and $\alpha_m(y_o^+ = 100)$, respectively. In other words, α_{add} converges from the SIAs of attached eddies with wall-normal height approximately 100 in viscous units to the mean SIA at $y_o^+ = 100$. This observation can be explained through the prism of the hierarchical attached eddies in high-Reynolds-number wall turbulence. The increase of y_o^+ indicates that $\tau'^+_{x,L}(y_s^+) - \tau'^+_{x,L}(y_o^+)$ and $u'^+_W(y_s^+) - u'^+_W(y_o^+)$ are contributed by more and more wall-attached eddies with their normal heights larger than y_s^+, and gradually become equal to $\tau'^+_{x,L}(y_s^+)$ and $u'^+_W(y_s^+)$, respectively, when y_o^+ approaches h^+. Thus R_{add} would also converge gradually to $R_{\tau'_{x,L} u'_W}$ in (4.2), and α_{add} converges to α_m and $\alpha_{SSE,m}$ concurrently.
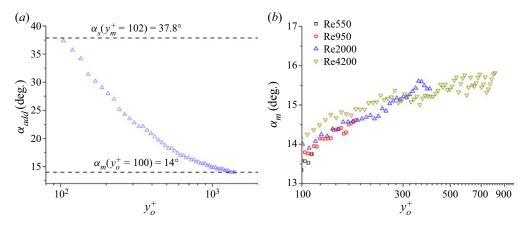
Figure 10. (*a*) Variations of the additive SIA α_{add} as a function of y_o^+ for Re2000. (*b*) The mean SIAs α_m as functions of y_o^+ for all cases.

Additionally, this study helps us to understand the variation tendency of α_m. Figure 10(*b*) plots the variations of α_m for all cases. It is observed clearly that α_m increases continuously with y_o^+. Taking Re2000 as an example, α_m increases from $14°$ for y_s^+ to $15.3°$ for y_e^+. Increasing y_o^+ implies that fewer and fewer wall-attached eddies contribute to u'. In this way, α_m would converge to α_s as y_o^+ increases, albeit more slowly.

4.3. *Scale-dependent inclination angles of wall-attached eddies*

An alternative approach for calculating the scale-dependent inclination angle (SDIA) has been reported by Baars *et al.* (2016). The following are the primary processes and outcomes. The scale-specific phase between u' at y^+ and y_o^+ can be estimated as

$$\Phi(\lambda_x) = \arctan \left\{ \frac{\text{Im} \left[\phi_{u_o' u'} \left(\lambda_x, y^+, y_o^+ \right) \right]}{\text{Re} \left[\phi_{u_o' u'} \left(\lambda_x, y^+, y_o^+ \right) \right]} \right\}, \tag{4.5}$$

where $\text{Im}(\cdot)$ and $\text{Re}(\cdot)$ denote the imaginary and real parts of $\phi_{u_o' u'}$, namely, the numerator of (2.2). The scale-dependent streamwise shift can be calculated as

$$l(\lambda_x) = \frac{\Phi(\lambda_x) \lambda_x}{2\pi}. \tag{4.6}$$

Accordingly, the SDIA can be estimated as

$$\alpha_{sd}(\lambda_x) = \arctan \left(\frac{y_o - y}{l(\lambda_x)} \right). \tag{4.7}$$

A positive α_{sd} value corresponds to a spatially forward-leaning structure.

Figure 11 shows the SDIAs as functions of λ_x/y_o for three selected wall-normal positions in the case Re2000. For $\lambda_x/y_o > 18$, the SDIAs of the large-scale motions are shown to be approximately equal to $14°$. (in fact, this is not the real SIA of the large-scale wall-attached structures, according to the study of Deshpande *et al.* 2019.) However, for the smaller length scales, the SDIAs tend to be negative and vary rapidly with λ_x/y_o. This is the range of self-similar structures reported by previous studies, especially those with $\lambda_x/y_o = 14$ (Baars *et al.* 2017; Baidya *et al.* 2019). Similar results have also been
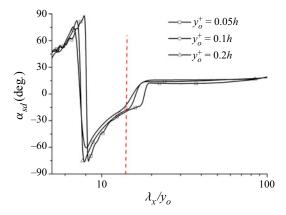
946 A49-14

Figure 11. Variations of the scale-dependent inclination angles for three selected wall-normal positions in the case Re2000. The vertical line denotes $\lambda_x/y_o = 14$.
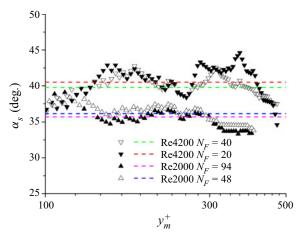

Figure 12. Plots of α_s as functions of y_m^+ for the cases Re2000 and Re4200 with different N_F. The dashed lines denote the mean value of α_s in the logarithmic region.

reported by Baars *et al.* (2016) (see figure 5 of their paper). It indicates that the phase spectrum shown in figure 11 cannot be interpreted with any physical relevance at these scales, as the scale-specific phases of them are random indeed. The contamination from the detached eddies with random orientations could be the source of this problem. This is the main purpose of the present study, i.e. to eliminate the corruption caused by the wall-detached motions and measure appropriately the SIAs of the wall-attached eddies at a certain wall-normal height.

5. Concluding remarks

In the present study, we develop a methodology to assess the streamwise inclination angles of the wall-attached eddies at a given wall-normal height in turbulent channel flows, by coupling the spectral stochastic estimation with the attached-eddy hypothesis. Our results show, for the first time, that the SIAs of the attached eddies are Reynolds-number-dependent in low and medium Reynolds numbers, and tend to be

consistent with the theoretical prediction (i.e. $\alpha_s = 45°$) as Reynolds number increases. We further reveal that the mean SIA reported by vast previous studies are the outcomes of the additive effect contributed by multi-scale attached eddies.

The attached-eddy model has been the guidance for the reconstruction of the velocity field in wall turbulence (Perry & Marusic 1995; Baidya *et al.* 2017; Chandran *et al.* 2017). Hierarchical vortex packets that consist of Λ-vortices with $\alpha_s = 45°$ are distributed on the wall surface to mimic the attached eddies. The present results suggest that a lower SIA of representative structures might be helpful for a more accurate reconstruction when the Reynolds number is not high enough. Moreover, within the state-of-the-art wall-modelled large-eddy simulation (WMLES) framework, one may estimate the instantaneous τ_x based on the velocities carried by the log region eddies (Fu *et al.* 2021; Fu, Bose & Moin 2022). The Reynolds number dependence of SIAs of these eddies should be accounted for by an advanced model in this sense.

Declaration of interests. The authors report no conflict of interest.

Author ORCIDs.

Cheng Cheng https://orcid.org/0000-0002-7961-793X;

Lin Fu https://orcid.org/0000-0001-8979-8415.

Appendix. Statistic sensitivity to N_F

The influences of the number of instantaneous flow fields for accumulating statistics are examined. Figure 12 shows the effect of N_F on the statistic α_s for the cases Re2000 and Re4200. Alteration of the statistical samples mainly affects the relative standard deviations (RSDs) of the results. To be specific, when N_F increases from 48 to 94, RSD decreases from 3.9 % to 3.3 % for Re2000; but for Re4200, RSD decreases from 6.5 % to 3.7 % when N_F increases from 20 to 40. Given the fact that the case Re4200 has limited domain size, raising N_F can effectively reduce the wiggles in the outputs. Nevertheless, the mean value of α_s in the logarithmic region seems to be insensitive to N_F.

REFERENCES

ADRIAN, R.J. 1979 Conditional eddies in isotropic turbulence. *Phys. Fluids* **22** (11), 2065–2070.

ADRIAN, R.J., MEINHART, C.D. & TOMKINS, C.D. 2000 Vortex organization in the outer region of the turbulent boundary layer. *J. Fluid Mech.* **422**, 1–54.

BAARS, W.J, HUTCHINS, N. & MARUSIC, I. 2016 Spectral stochastic estimation of high-Reynolds-number wall-bounded turbulence for a refined inner–outer interaction model. *Phys. Rev. Fluids* **1** (5), 054406.

BAARS, W.J., HUTCHINS, N. & MARUSIC, I. 2017 Self-similarity of wall-attached turbulence in boundary layers. *J. Fluid Mech.* **823**, R2.

BAARS, W.J. & MARUSIC, I. 2020*a* Data-driven decomposition of the streamwise turbulence kinetic energy in boundary layers. Part 1. Energy spectra. *J. Fluid Mech.* **882**, A25.

BAARS, W.J. & MARUSIC, I. 2020*b* Data-driven decomposition of the streamwise turbulence kinetic energy in boundary layers. Part 2. Integrated energy and a_1. *J. Fluid Mech.* **882**, A26.

BAIDYA, R., *et al.* 2019 Simultaneous skin friction and velocity measurements in high Reynolds number pipe and boundary layer flows. *J. Fluid Mech.* **871**, 377–400.

BAIDYA, R., PHILIP, J., HUTCHINS, N., MONTY, J.P. & MARUSIC, I. 2017 Distance-from-the-wall scaling of turbulent motions in wall-bounded flows. *Phys. Fluids* **29** (2), 020712.

BOPPE, R.S., NEU, W.L. & SHUAI, H. 1999 Large-scale motions in the marine atmospheric surface layer. *Boundary-Layer Meteorol.* **92** (2), 165–183.

BROWN, G.L. & THOMAS, A.S. 1977 Large structure in a turbulent boundary layer. *Phys. Fluids* **20** (10), S243–S252.

CARPER, M.A. & PORTÉ-AGEL, F. 2004 The role of coherent structures in subfilter-scale dissipation of turbulence measured in the atmospheric surface layer. *J. Turbul.* **5** (1), 32–55.

CHANDRAN, D., BAIDYA, R., MONTY, J.P. & MARUSIC, I. 2017 Two-dimensional energy spectra in high-Reynolds-number turbulent boundary layers. *J. Fluid Mech.* **826**, R1.

CHENG, C. & FU, L. 2022 Consistency between the attached eddy model and the inner outer interaction model: a study of streamwise wall shear stress fluctuations in a turbulent channel flow. *J. Fluid Mech.* **942**, R9.

CHENG, C., LI, W., LOZANO-DURÁN, A. & LIU, H. 2019 Identity of attached eddies in turbulent channel flows with bidimensional empirical mode decomposition. *J. Fluid Mech.* **870**, 1037–1071.

CHENG, C., LI, W., LOZANO-DURÁN, A. & LIU, H. 2020*a* On the structure of streamwise wall-shear stress fluctuations in turbulent channel flows. *J. Fluid Mech.* **903**, A29.

CHENG, C., LI, W., LOZANO-DURÁN, A. & LIU, H. 2020*b* Uncovering Townsend wall-attached eddies in low-Reynolds-number wall turbulence. *J. Fluid Mech.* **889**, A29.

CHO, M., HWANG, Y. & CHOI, H. 2018 Scale interactions and spectral energy transfer in turbulent channel flow. *J. Fluid Mech.* **854**, 474–504.

CHRISTENSEN, K.T. & ADRIAN, R.J. 2001 Statistical evidence of hairpin vortex packets in wall turbulence. *J. Fluid Mech.* **431**, 433–443.

DE SILVA, C.M., MARUSIC, I. & HUTCHINS, N. 2016 Uniform momentum zones in turbulent boundary layers. *J. Fluid Mech.* **786**, 309–331.

DEL ÁLAMO, J.C. & JIMÉNEZ, J. 2003 Spectra of the very large anisotropic scales in turbulent channels. *Phys. Fluids* **15** (6), L41–L44.

DEL ÁLAMO, J.C., JIMÉNEZ, J., ZANDONADE, P. & MOSER, R.D. 2004 Scaling of the energy spectra of turbulent channels. *J. Fluid Mech.* **500**, 135–144.

DESHPANDE, R., MONTY, J.P. & MARUSIC, I. 2019 Streamwise inclination angle of large wall-attached structures in turbulent boundary layers. *J. Fluid Mech.* **877**, R4.

DESHPANDE, R., MONTY, J.P. & MARUSIC, I. 2021 Active and inactive components of the streamwise velocity in wall-bounded turbulence. *J. Fluid Mech.* **914**, A5.

FU, L., BOSE, S. & MOIN, P. 2022 Prediction of aerothermal characteristics of a generic hypersonic inlet flow. *Theor. Comput. Fluid Dyn.* **36** (2), 345–368.

FU, L., KARP, M., BOSE, S.T., MOIN, P. & URZAY, J. 2021 Shock-induced heating and transition to turbulence in a hypersonic boundary layer. *J. Fluid Mech.* **909**, A8.

HOYAS, S. & JIMÉNEZ, J. 2006 Scaling of the velocity fluctuations in turbulent channels up to $Re_\tau = 2003$. *Phys. Fluids* **18** (1), 011702.

HU, R., YANG, X.I.A. & ZHENG, X. 2020 Wall-attached and wall-detached eddies in wall-bounded turbulent flows. *J. Fluid Mech.* **885**, A30.

HWANG, Y. 2015 Statistical structure of self-sustaining attached eddies in turbulent channel flow. *J. Fluid Mech.* **767**, 254–289.

HWANG, J., LEE, J. & SUNG, H. 2020 Statistical behaviour of self-similar structures in canonical wall turbulence. *J. Fluid Mech.* **905**, A6.

HWANG, J. & SUNG, H.J. 2018 Wall-attached structures of velocity fluctuations in a turbulent boundary layer. *J. Fluid Mech.* **856**, 958–983.

JIMÉNEZ, J. 2018 Coherent structures in wall-bounded turbulence. *J. Fluid Mech.* **842**, P1.

KOVASZNAY, L.S.G., KIBENS, V. & BLACKWELDER, R.F. 1970 Large-scale motion in the intermittent region of a turbulent boundary layer. *J Fluid Mech.* **41** (2), 283–325.

LOZANO-DURÁN, A. & JIMÉNEZ, J. 2014 Effect of the computational domain on direct simulations of turbulent channels up to $Re_\tau = 4200$. *Phys. Fluids* **26** (1), 011702.

MARUSIC, I. 2001 On the role of large-scale structures in wall turbulence. *Phys. Fluids* **13** (3), 735–743.

MARUSIC, I. & HEUER, W.D.C. 2007 Reynolds number invariance of the structure inclination angle in wall turbulence. *Phys. Rev. Lett.* **99** (11), 114504.

MARUSIC, I., MATHIS, R. & HUTCHINS, N. 2010 Predictive model for wall-bounded turbulent flow. *Science* **329** (5988), 193–196.

MARUSIC, I. & MONTY, J.P. 2019 Attached eddy model of wall turbulence. *Annu. Rev. Fluid Mech.* **51**, 49–74.

MARUSIC, I., MONTY, J.P., HULTMARK, M. & SMITS, A.J. 2013 On the logarithmic region in wall turbulence. *J. Fluid Mech.* **716**, R3.

MARUSIC, I. & PERRY, A.E. 1995 A wall-wake model for the turbulence structure of boundary layers. Part 2. Further experimental support. *J. Fluid Mech.* **298**, 389–407.

MOIN, P. & KIM, J. 1985 The structure of the vorticity field in turbulent channel flow. Part 1. Analysis of instantaneous fields and statistical correlations. *J. Fluid Mech.* **155**, 441–464.

MOURI, H. 2017 Two-point correlation in wall turbulence according to the attached-eddy hypothesis. *J. Fluid Mech.* **821**, 343–357.

PERRY, A.E. & CHONG, M.S. 1982 On the mechanism of wall turbulence. *J. Fluid Mech.* **119** (119), 173–217.

PERRY, A.E., HENBEST, S. & CHONG, M.S. 1986 A theoretical and experimental study of wall turbulence. *J. Fluid Mech.* **165**, 163–199.

PERRY, A.E. & MARUSIC, I. 1995 A wall-wake model for the turbulence structure of boundary layers. Part 1. Extension of the attached eddy hypothesis. *J. Fluid Mech.* **298** (298), 361–388.

PERRY, A.E., UDDIN, A.K.M. & MARUSIC, I. 1992 An experimental and computational study on the orientation of attached eddies in turbulent boundary layers. In *Proceedings of the 11th Australasian Fluid Mechanics Conference, Hobart, Australia.*

TOWNSEND, A.A. 1976 *The Structure of Turbulent Shear Flow*, 2nd edn. Cambridge University Press.

WANG, L., HU, R. & ZHENG, X. 2021 A scaling improved inner–outer decomposition of near-wall turbulent motions. *Phys. Fluids* **33** (4), 045120.

WOODCOCK, J.D. & MARUSIC, I. 2015 The statistical behaviour of attached eddies. *Phys. Fluids* **27** (1), 97–120.

YANG, X.I.A. & LOZANO-DURÁN, A. 2017 A multifractal model for the momentum transfer process in wall-bounded flows. *J. Fluid Mech.* **824**, R2.

YANG, X.I.A., MARUSIC, I. & MENEVEAU, C. 2016 Moment generating functions and scaling laws in the inertial layer of turbulent wall-bounded flows. *J. Fluid Mech.* **791**, R2.

YOON, M., HWANG, J., YANG, J. & SUNG, H.J. 2020 Wall-attached structures of streamwise velocity fluctuations in an adverse-pressure-gradient turbulent boundary layer. *J. Fluid Mech.* **885**, A12.